Compact real-time online oil spill detection system based on surface plasmon resonance

Zheng Yan[1], Sun Yufeng[1], Xing Liyun[1,2], Dai Guangbin[1,3], Chang Tianying[1,3], Xia Liangping[3], Wang Min[1], Lang Jinpeng[1],Cui Hongliang[1,3]

(1. College of Instrumentation & Electrical Engineering, Jilin University, Changchun 130021, China;
2. College of Electrical and Information Engineering, Beihua University, Jilin 130000, China;
3. Research Center for Terahertz Technology, Chongqing Institute of Green and Intelligent Technology, Chinese Academy of Sciences, Chongqing 400714, China)

Abstract: The design and preliminary investigation of a real-time, online, all-weather accurate monitoring system for the early detection and warning of difficult-to-detect, inchoate, small-area oil spills were presented. The scheme is based on a miniaturized surface plasmon resonance (SPR) device. The system used a light source with a non-scanning angle modulation to ensure that the light cover the incident angle range of variation related to the samples under test. With a fixed range of sample refractive indices, corresponding to most of the known crude and refined oil products, the parameters for the detector through optimization of the central wavelength and the incident angle of the light source were obtained, as well as related parameters of the prism by a combinational simulation using commercial software packages MATLAB and ZEMAX. Through modeling and simulation, followed by preliminary experiments a basic model for the system feasibility was arrived for the proposed purpose.

Key words: surface plasmon resonance; MATLAB; ZEMAX; simulation; optimization
CLC number: TN253;TM452.94 **Document code:** A **Article ID:** 1007-2276(2015)11-3446-08

基于表面等离子体共振原理的小型化实时在线海上溢油监测系统

郑 妍[1],孙玉锋[1],邢砾云[1,2],代广斌[1,3],常天英[1,3],夏良平[3],王 敏[1],郎金鹏[1],崔洪亮[1,3]

(1. 吉林大学 仪器科学与电气工程学院,吉林 长春 130021;
2. 北华大学 电气信息工程学院,吉林 吉林 132013;
3. 中国科学院重庆绿色智能技术研究院 太赫兹技术研究中心,重庆 400714)

收稿日期:2015-03-11; **修订日期**:2015-04-20
基金项目:国家科技支撑计划项目(2012BAK04B03);海洋公益性行业科研专项经费项目(201405026-01);重庆市科委基础研究计划重大项目资助(cstc2013jcyjC00001)
作者简介:郑妍(1990-),女,硕士生,主要从事光纤 SPR 传感器、棱镜 SPR 传感器、纳米光学与纳米电子学方面的研究工作。Email: zhengyan400356@sina.cn
导师简介:崔洪亮(1956-),男,国家“千人计划”特聘教授,博士生导师,博士,主要从事光纤通信和传感、固态电子及半导体物理和器件、THz 科学技术及应用、纳米光学和纳米电子学等方面的研究工作。Email: hcui@jlu.edu.cn
通讯作者:常天英(1981-),女,博士,主要从事光纤传感技术与应用、光纤分布式传感(拉曼、布里渊技术、BOTDR)等方面的研究工作。Email: tchang@jlu.edu.cn

摘 要：为了对不易被发现的早期小面积溢油进行高精度、全天候、实时在线的监测，以达到早发现、早预警、早处理的目的，提出了基于表面等离子体共振(surface plasmon resonance，SPR)技术的小型化实时在线海上溢油检测系统的设计思想，系统拟采用入射光源为非扫描的角度调制型方式，目的是便于光线完全覆盖待测样品检测时所需的入射角度范围。对大量的原油和石油样品的折射率进行检测确定其范围，再通过 MATLAB 与 ZEMAX 模拟仿真结合，得到了光源最优化的中心波长、入射角度范围以及棱镜的相关参数，并确定出探测器的相关指标。最终通过建模与仿真，验证了系统装置的可行性，并得出了初步试验方案。

关键词：表面等离子体共振；　MATLAB；　ZEMAX；　仿真；　优化

0 Introduction

Surface plasmon resonance (SPR) technology, based mainly on ingenious uses of surface plasmon waves (SPW), is a detection technology to realize the optoelectronic phenomenon related to the test substance of the sensing medium surface by analyzing the changes in optical parameters. In 1902, Wood first found that SPR was the collective excitation of the metal surface electron ensemble arisen from the optical excitation. In the 1970s, Otto and Kretschmann further demonstrated the potential of SPR sensing technology in the thin film configuration and its ability to monitor opto-electronic processes at the metal interface, which has laid a firm theoretical foundation for the SPR sensing technology[2-3]. The technology has generated much attention because of advantages such as its detection speed, sensitivity, and that it requires samples without tags, without separation and purification, and its ability for real-time, dynamic monitoring[4-5]. It has been applied widely in the field of biological and chemical analyses, medical diagnostics, pharmaceutical processing, and food and environmental monitoring[6-8]. Small, portable SPR biosensors have emerged and been commercialized abroad, although related research, especially those toward practical applications in environmental monitoring in our country is still in its infancy. Therefore it is promising and meaningful to develop a compact SPR oil spill detection system in real-time online monitoring, for the purpose of prevention, early warning and emergency response of small-area oil spills.

This work is concerned with the development of a compact real-time online SPR oil spill detection system to realize the precision detection and emergency response of the important and sensitive waters (e.g. subsea oil spill area, submarine pipeline spill area). Currently, oil spill monitoring relies on satellite and aerial remote sensing, remote monitoring of shipping lanes by sentinel surveillance and tracking buoys. But these technologies are not early detection[9-11]. With the proposed SPR detection system, we demonstrate the feasibility for real-time online oil spill detection. In the remaining parts of the present paper, we present technical details and the selection and analysis of devices of key modules for the implementation of the system, and discuss placement of the package, formation of distributed networks, and the merging of multi-sensor data to realize the monitoring of oil spills in real time. The implementation of the system will make it possible to track the spill position and scale, its drift velocity, trajectory and direction to provide such important information as the leak location and its degree of severity.

1 Theoretical background and design of the system

1.1 Principle

The compact, real-time, online oil spill detected device is based on the angle-modulated non-scanning SPR with the coupler-model structure of a Kretschmann prism, in which non-scanning mode modulation is used as the incident light is scattered while the wavelength is fixed. This modulation scheme ensures that the range of incident

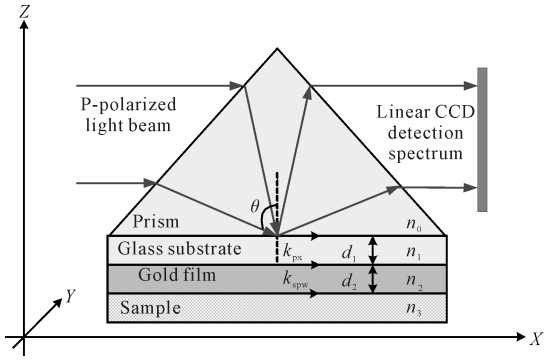

Fig.1 Non-scanning, angle modulated SPR sensor based on a coupler model structure with Kretschmann prism

angles be completely covered. The corresponding optimized system parameters are shown in Figure 1.

The necessary conditions for optical excitations of SPR are as follows: (1) The incident light must be P-polarized, as the s-polarized light wave has its electric field vector perpendicular to the interface and can not excite SPW resonance. (2) The wave vector of the incident light matches the wave vector of the SPW to transfer momentum to the latter. (3) The index of refraction of the prism is such that the incident light undergoes total internal reflection at the prism-metal film interface, producing an evanescent wave on the metal side of the interface. (4) The thickness of the metal layer is less than the penetration depth of the evanescent wave, so that the latter can reach the interface between the metal layer and the sample, whereby it excites the SPR, which reveals the index of refraction of the sample, on which the detection scheme is based.

1.2 System design

We envision that our system will comprise several modules each with specialized functions. Specifically, the circulation and regeneration module is designed for the handling of the sample and cleaning and regenerating of the detection surface; the "heart" of the system, the sensor module performs the core function of sample detection; the positioning and communication module provide the system with positioning and communication capabilities; while the software control module functions as the "brain" of the system, and finally the power module supplies power to the entire system. Figure 2 is a schematic

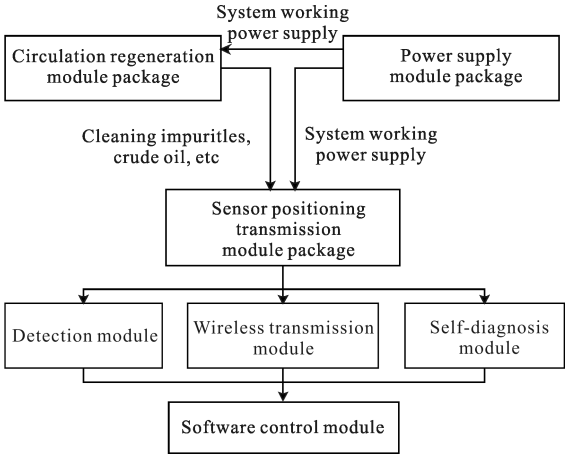

Fig.2 Compact SPR oil spill detection system diagram

diagram of the compact SPR oil spill detection system.

1.3 System process structure

Our approach to design the oil spill detection system consists of several steps, as shown in Figure 3. First, through a systematic composition and measurements of a variety of liquid hydrocarbons blends(mostly crude oil and refined oil products) composition testing, we determine the range of variation of refractive index to be effectively detected by the sensor. Secondly, we determine the center wavelength of the light source and the desired range of angle of incidence according to the principle of surface plasmon resonance, taking into account the refractive index range of the samples to be detected. The range of the index of refraction of the target samples also affects the range of index of refraction of (thereby the material of) the prism. With the former decided, now the choice of the material of the prism can be made.

Once the center wavelength and angle of incidence of light, as well as the prism material are determined, ZEMAX optical ray tracing simulation is carried out to optimize shape and geometry of the prism including each side length, and each internal angle of the prism.

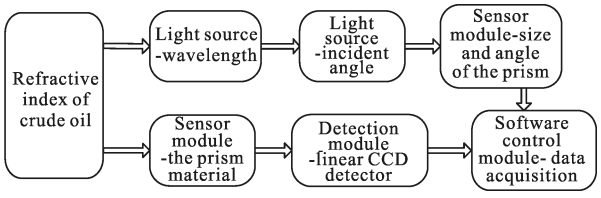

Fig.3 Flowchart of the system processing structure

Simultaneously we also determine the thicknesses of the gold film and the sensor glass slides required to obtain a configuration that meet the detection requirements for depth and breadth. Finally, the determination of all the above parameters can be considered jointly with a linear CCD array detector and computer data acquisition and processing parts of the control module.

2 Theoretical analysis

Next we employ Fresnel′s formula[12] to obtain the reflectivity of the four-layer Kretchmann structure. Assuming the dielectric constants of the prism, the sensing wave plate, the gold film, and the sample are ε_0, ε_1, ε_2 and ε_3 respectively. The components of the wave vectors of the light in the z-direction in the sensor glass slide, the gold film, and the medium to be tested are k_{pz1}, k_{pz2} and k_{pz3}, respectively. First we can calculate the reflection coefficients between the adjacent layers:

$$r_{p12}=\frac{E'_{1p}}{E_{1p}}=\frac{n_2\cos\theta_1-n_1\cos\theta_2}{n_2\cos\theta_1+n_1\cos\theta_2}=\frac{\varepsilon_2 k_{pz1}-\varepsilon_1 k_{pz2}}{\varepsilon_2 k_{pz1}-\varepsilon_1 k_{pz2}}$$

$$r_{p23}=\frac{E'_{2p}}{E_{2p}}=\frac{n_3\cos\theta_2-n_2\cos\theta_3}{n_3\cos\theta_2+n_2\cos\theta_3}=\frac{\varepsilon_3 k_{pz2}-\varepsilon_2 k_{pz3}}{\varepsilon_3 k_{pz2}-\varepsilon_2 k_{pz3}}$$

The incident light wave vector in the x direction is $k_{px}=n_0\frac{w}{c}\sin\theta$.

Therefore, the wave vector in the z-direction can be written as $k_{pzm}=\sqrt{\frac{w^2}{c^2}\varepsilon_m-k_{px}^2}=\sqrt{\frac{w^2(\varepsilon_m-n^2\sin^2\theta)}{c^2}}$.

And the reflectivity is given by

$$R=|r_{13}|^2=\left|\frac{r_{12}+r_{23}e^{i2k_{pz2}d_2}}{1+r_{12}r_{23}e^{i2k_{pz2}d_2}}\right|^2$$

where d_1 and d_2 are the thicknesses of the sensing slide and the gold film respectively, as the materials making up the prism and the wave plate are the same, d_1 can be neglected, and as a result, $r_{01}=0$.

Using angle modulation and fixing the wavelength of the incident light, we can simulate the variations of the light intensity within a certain range of incident angle, whose upper and lower limits are to be determined through an optimization of the system parameters.

3 Design simulation

3.1 MATLAB calculation

In the SPR model, we firstly set the refractive indexes of varied layers, according to the Fresnel formulas, then took advantage of the model which combined both MATLAB and ZEMAX software to obtain the required parameters in the practical monitoring, such as, center wavelength and linewidth of the laser source, the thickness of the gold film, the material, the size and the refractive index of the prism.

The refractive indices of marine spilled oil lie between 1.40 and 1.55 according to available data. For example, a common type crude oil sample obtained from SINOPEC's Shengli Oilfield has a refractive index 1.5299 by repeated measurements with an Abbe refractometer (RA-600, Electronic Industrial Co., Ltd, Kyoto, Japan), whose nominal accuracy is ±0.000 1.

3.1.1 Refractive index of the prism

Once the refractive index range of at sea oil spill is determined (1.40-1.55), we can proceed with the design of the system. However, to guard against possible presence of higher refractive index crude oil, we will design the system with a maximum sample index of refraction of about 1.80 (instead of 1.55). According to the material parameters and the refractive index of available glass materials for making prisms, we select the dense flint glass ZF13 whose refractive index is 1.784 72 for the prism. As shown in Figures 4 and 5, with the refractive index of 1.784 72 for the prism, the range of the refractive index and the corresponding resonance angle, can all be detected by the system.

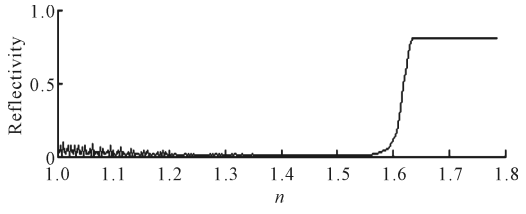

Fig.4 Reflectivity of the sample as a function of its refractive index

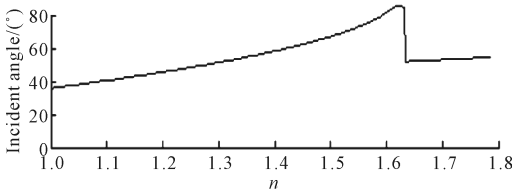

Fig.5 Incident angle of the sensor as a function of the refractive index of the sample

3.1.2 Light source

We employ MATLAB for simulation to obtain the relationship between the sample refractive index and the resonance wavelength, with the result being shown in Figure 6. Simultaneously, through an analysis of the data presented in Figure 6, with the refractive index of the sample falling between 1.40 –1.55, the corresponding center wavelength of the incident light source is determined to be between 565.3–917.5 nm. The spectral range of the light source covers almost the entire visible band, although an analysis using the center wavelength of the red light can completely cover the refractive index of the sample family (1.40–1.55).

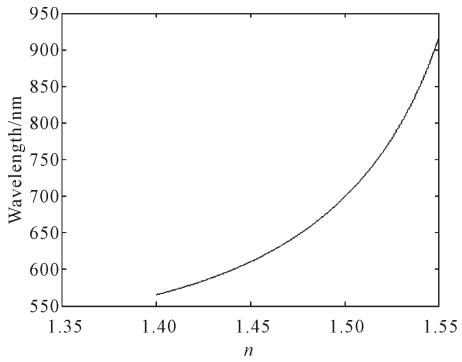

Fig.6 Relationship between the resonance wavelength and the sample refractive index

With the given refractive indices of the samples, we can determine relationship between the resonance angle and the resonance wavelength, as shown in Figure 7. By an analysis at the resonance wavelength of 635.1 nm, we find the resonance angles are 58.29°, 65.14°, 70.51°, and 73.19°, respectively, corresponding to the sample refractive index of 1.40, 1.48, 1.529 9, and 1.55, respectively. Accordingly, the optimal center wavelength of the incident light is chosen to be 635 nm.

On the other hand, given the center wavelength of the

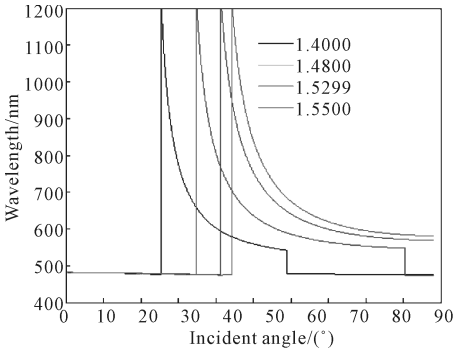

Fig.7 Relationship between incident angle and the resonance wavelength for several values of the index of refraction of the samples

incident light, i.e., 635 nm, we can obtain the relationship between the sample refractive index and the incident angle, as shown in Figure 8. Likewise, with the center wavelength at 635 nm, we obtain the relationship between the resonance angle of incidence and refractive index of the sample, as shown in Figure 9. By analyzing the two graphs presented in Figures 8–9, all the resonance angle can be obtained when the incident angle is between 58° and 74°. For instance, the resonance angles are 58.31°, 65.34°, 70.55°, and 73.06° with respect to the sample refractive index 1.40, 1.48, 1.529 9, and 1.55, respectively.

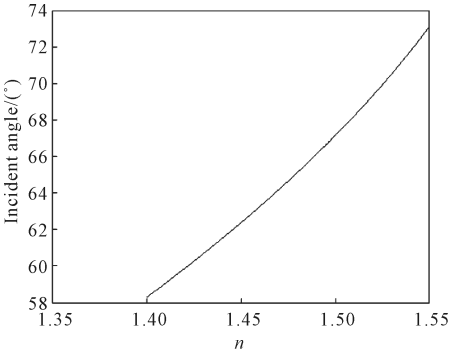

Fig.8 Relationship between incident angle and refractive index of the sample with a given central wavelength (635 nm)

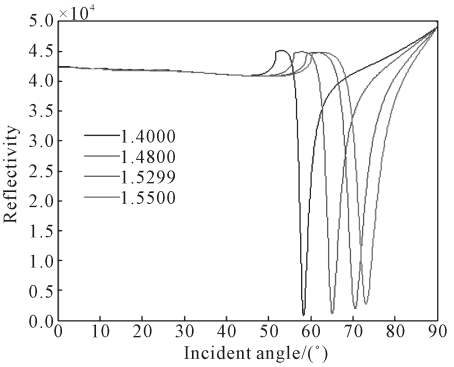

Fig.9 Reflectivity as a function of the incident angle

The inverse relations can also be obtained. Figures 10-12 show typical data sets.

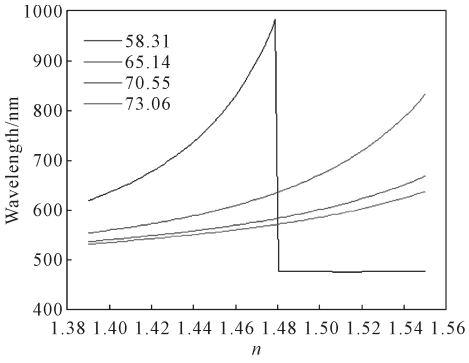

Fig.10 Resonant wavelength as a function of the refractive index of the sample for several incident angles

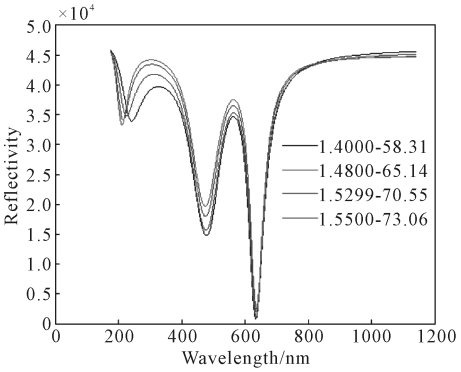

Fig.11 Relationship between reflectivity and the resonance wavelength for various values of the refractive index of the sample and the incident angle

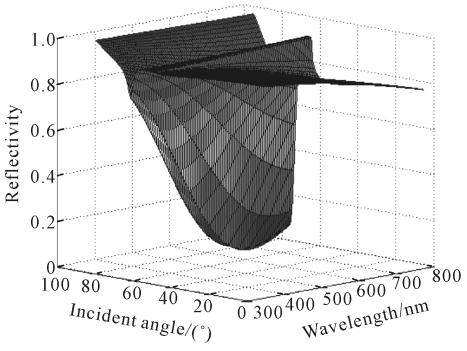

Fig.12 Relations among the resonance wavelength, the reflectivity and the incident angle

According to the analyses of all the graphs presented above, one can get the refractive index of all tested samples of crude oil when the angle of incidence of the light source lies between 58° and 74°. Along with Snell's law of refraction, we conclude that the emission angle of the incident light should not be less than 30°.

Therefore, we choose a semiconductor laser module as the light source, with its central wavelength at 635 nm in red light band, emission angle less than 30°, and output power below 5 mW.

3.1.3 Thickness of the gold film

For the case of the non-scanning angle modulation type SPR sensor, different light resonant wavelengths correspond to their respectively suitable gold film thicknesses. Consider the typical situation where the central wavelength is 635 nm, the refractive index of the crude oil sample is, e.g., 1.529 9, and the incident angle is 70.55°, according to the classical Drude metal electron gas model[13-14], one can derive the gold complex dielectric constant to be −13.174 8+1.257 5i. We can then obtain the relation between the gold film thickness and reflectivity, as shown in Figure 13, and the three-dimensional plot of the relationship among the resonance wavelength, the gold film thickness and the reflectivity, as shown in Figure 14.

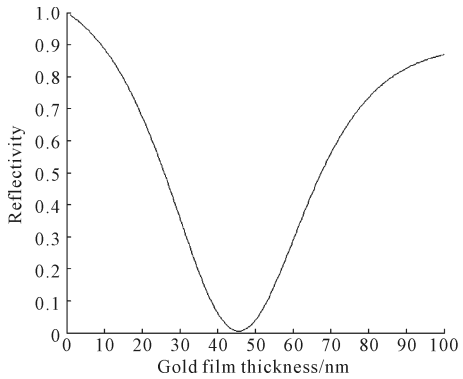

Fig.13 Relation between the gold film thickness and the reflectivity

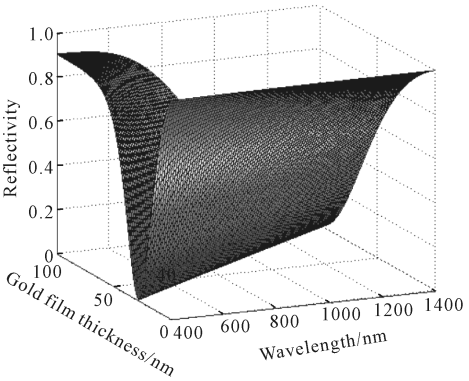

Fig.14 Reflectivity as a function of the resonance wavelength and the gold film thickness

According to the above analysis, there exists an optimal thickness for the gold film value in the visible band, corresponding to the optimized sensitivity. When the central wavelength is 635 nm, the optimized gold film thickness is 46 nm.

3.2 ZEMAX simulation

ZEMAX is often used to obtain the light path design, optimization, analysis and estimation of tolerances in the optical system testing and simulation, with its output in the form of some charts and data, followed by data analysis and processing, which is not always easy and straightforward. Therefore, having the powerful scientific computing capabilities of MATLAB and optical design abilities of ZEMAX connected to each other to transfer data, can help to fully realize the advantage of the software packages and improve efficiency.

In this work we design the structure of the prism-based system sensing module, using ZEMAX and MATLAB to simulate and compute the combined results for the Quadrilateral-hexahedral prism, which is conducive to miniaturization of the structural design. The reflectivity of the coated side of the prism can reach 90% at the inner reflecting surface, so that the light source and detector can be located in the same plane. Moreover, the control circuit is designed to reduce the required size, and the encapsulated equipment volume is greatly reduced. A typical ZEMAX simulation is shown in Figure 15.

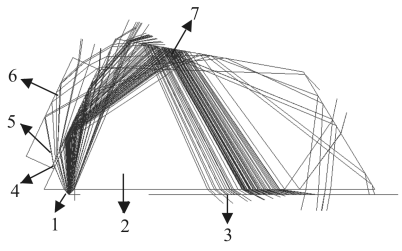

1: Light source; 2: Prism; 3: Linear CCD detector array; 4: Refractive index matching glue; 5: Gold film coated sensor glass slide; 6: Crude oil sample; 7: Internal reflector

Fig.15 Ray tracing from ZEMAX simulation of the optical sensing system

Simulation proves that the optimal shape of the prism is Quadrilateral-hexahedral, with the sizes of the prism given below. The bottom edge length is 60 mm and it is the longest edge. The side with the gold film sensing slides length is 30.47 mm and has an angle of 65° with respect to the bottom edge. The side with the internal reflector is 25.47 mm and the remaining side is 25.47 mm. All the above lengths are determined with an accuracy of +/−0.01 mm.

Figure 15 shows that the light impinges from the front entrance of the prism. To ensure that the light covers the range of the refractive index of the crude oil samples, we will use a wide beam light source with large divergence angles. This also ensures that the detector array is covered completely, which is confirm by a calculation of the incidence angles for the entire beam range.

Crude oil is composed of a variety of hydrocarbons with different physical properties, including its varied refractive indices. The simulation takes the crude oil refractive index of 1.529 9, it invariably generates stray light spilling from the edge of the prism, which does not belong to the detection range. After detailed analysis, we ascertained that the stray light generated does not affect the detection result, as the light associated with the surface plasmon resonance phenomenon will suffer a total internal reflection (TIR) on the gold film sensor glass slide 5, which has been closely attached to the prism 2 by the matching glue (liquid) adhesive 4. The light beam reaches the internal reflector coated with the total internal reflection coating will also undergo a total internal reflection, with the reflected light beam going to the bottom of the rear end of the prism, subsequently received by the linear CCD detector array.

The linear CCD detector array (TCD1501, from TOSHIBA company) with high precision (Pixel pitch is 7 μm) and high sensitivity (Saturated exposure is 0.037lx·s) consists of 5 000 pixels, which has been modified from a wired transmission mode into a wireless transmission mode. With the matched driver, it can acquire image data with a high efficiency. Furthermore, a positioning device module and a test module have been embedded in the hardware circuit board of the CCD array detector to get the real-time state of the system with a higher efficiency and to ensure the operational stability of the system.

4 Conclusion

With the analysis of the compact real-time online oil spill detection system, which is based on the angle-modulated non-scanning SPR, with the coupler model structure of a Kretschmann prism, we first optimized the system design by simulation using MATLAB. We then acquired the optical simulated beam path through the combination of the data obtained above and the ZEMAX software. The optimal design of the optical sensing module and reduction of the model volume of overall the experimental system are achieved to miniaturize the oil spill detection system. This work provides an important basis for further experiments, such as the manipulation and building of the experiment devices, and helps for the implementation of the miniaturized real-time online oil spill system. The final system can provide for a real-time online, all-weather, continuous and monitor of otherwise undetectable trace amount, inchoate, small-area spills.

References:

[1] Wood R W. On a remarkable case of uneven distribution of light in a diffraction grating spectrum [J]. ***The London, Edinburgh, and Dublin Philosophical Magazine and Journal of Science***, 1902, 4(21): 396-402.

[2] Otto A. Excitation of nonradiative surface plasma waves in silver by the method of frustrated total reflection[J]. ***Zeitschrift Physik A Hadrons and Nuclei***, 1968, 216(4): 398-410.

[3] Kretschmann E, Raether H. Radiative decay of nonradiative surface plasmons excited by light (Surface plasma waves excitation by light and decay into photons applied to nonradiative modes) [J]. ***Zeitschrifl Fuer Naturforschung***, 1968, 23: 2135.

[4] Shagufta H K, Kriszta F, Kumar Raj, et al. A versatile method to measure the binding to basic proteins by surface Plasmon resonance [J]. ***Analytical Biochemistry***, 2012, 421 (2): 385-390.

[5] Deependra Tyagi, Javier Batista Perez, Amita Nand. Application of surface plasmon resonance imaging technique for iPSCs identification[J]. ***Science Bulletin***, 2015, 60(4): 483-485.

[6] Li Y, Liu X, Lin Z. Recent developments and applications of surface plasmon resonance biosensors for the detection of my cotoxins in foodstuffs[J]. ***Food Chemistry***, 2012, 132 (3): 1549-1554.

[7] Lee S J,Youn B S, Park J W, et al. ssDNA aptamer-based surface plasmon resonance biosensors for the detection of retinol binding protein 4 for the early diagnosis of type 2 diabetes [J]. ***Analytical Chemistry***, 2008, 80(1): 2867-2873.

[8] Andreea Olaru, Camelia Bala, Nicole Jaffrezic-Renault, et al. Surface plasmon resonance(SPR) biosensors in pharmaceutical analysis [J]. ***Critical Reviews in Analytical Chemistry***, 2015, 45(2): 97-105.

[9] Robert A Rose, Dirck Byler, Ron Eastman J, et al. Ten ways remote sensing can contribute to conservation [J]. ***Conservation Biology***, 2015, 29 (2): 350-359.

[10] Hu Jiachen, Wang Difeng. Monitoring method of ocean oil spilling based on remote sensing[J]. ***Environmental Protection Science***, 2014, 40(1): 68-73. (in Chinese)

[11] Klemas V. Tracking and monitoring oil slicks using remote sensing[C]//Baltic International Symposium(BALTIC), 2012: 1-7.

[12] Cheung M C, Chan H L, Zhou Q F. Characterization of barium titanate ceramic/ceramic nanocomposite films prepared by a SolGel process[J]. ***Nano Structure Materials***, 1999, 11 (7):837-844.

[13] Maxwell Garnett J C. Colours in metal glasses and in metallic films[J]. ***Proceedings of the Royal Society of London***, 1904, 73: 443-445.

[14] Li Y H, Lue J T. Dielectric constoits of single-wall carbon nanotubes at various frequencies[J]. ***Journal of Nanoscience and Nanotechnology***, 2007, 7: 3185-3188.